

# Evidence of fractional matching states in nanoperforated Nb thin film grown on porous silicon

M. Trezza<sup>1</sup>, C. Cirillo<sup>1</sup>, S. L. Prischepa<sup>2</sup> and C. Attanasio<sup>1,3</sup>

<sup>1</sup> Laboratorio Regionale SuperMat, CNR-INFM Salerno and Dipartimento di Fisica "E. R. Caianiello", Università degli Studi di Salerno, Baronissi (Sa) I-84081, Italy

<sup>2</sup> State University of Informatics and RadioElectronics, P. Brovka street 6, Minsk 220013, Belarus

<sup>3</sup> NANO-MATES, Research Centre for NANOMaterials and nanoTEchnology at Salerno University, Università degli Studi di Salerno, Fisciano, (Sa) I-84084, Italy

PACS 74.25.Fy { Transport properties of superconductors  
PACS 74.25.Qt { Vortex lattices, flux pinning, flux creep  
PACS 81.05.Rm { Porous materials

**Abstract.**—Resistive transitions have been measured on a perforated Nb thin film with a lattice of holes with the period of the order of ten nanometers. Bumps in the  $dR/dH$  versus  $H$  curves have been observed at the first matching field and its fractional values,  $1/4$ ,  $1/9$  and  $1/16$ . This effect has been related to different vortex lattice configurations made available by the underlying lattice of holes.

**Introduction.** { The nucleation of Abrikosov vortices [1] in the mixed state of type-II superconductors with periodic artificial pinning centers attracted a great attention since 1970's. Recent progress in the fabrication of nanostructures provides the possibility to realize superconducting thin films containing artificial defects as pinning sites with well-defined size, geometry and spatial arrangement [2,3]. Vortex pinning was extensively explored by many groups to develop a fundamental understanding of flux dynamics and for its relevance in applications which require enhancements of the critical current density. Thus, several types of artificial pinning centers, such as square, rectangular or triangular arrays, have been introduced in a controlled way in the superconducting films. In particular, the use of regular array of pinning centers such as antidots [2,4{6] or magnetic dots [3,7{9] brings to new commensurability effects, which give additional insight into the pinning properties of vortices. The most notable phenomenon for these studies is the so-called matching effect which occurs when the vortex lattice is commensurate with the periodic pinning array. This situation occurs, in particular, at fractional or integer values of the so-called first matching field  $H_1 = \phi_0/a_0^2$ , i.e., when the applied field  $H$  corresponds to one flux quantum,  $\phi_0 = h/2e$ , per unit cell area,  $a_0^2$ , of the pinning array. Here  $a_0$  is the lattice constant of the pinning arrangement. As a result, at

the matching field, the critical current density,  $J_c$ , is drastically enhanced [3,4,10] and moreover, as a consequence of the Little-Parks effect [11], the upper critical magnetic field is increased at the matching values. Recently antidot arrangements with a big variety of symmetries have been investigated. Matching effects have been reported in perforated Nb thin films for antidots lattices with short range order [12], or quasiperiodic veffold Penrose structures [13]. Moreover asymmetric pinning arrays have been suggested as superconducting rectifiers [14].

If the artificial structure of defects is created by lithographic technique, the matching fields are usually in the range of a few oersteds. For this reason, matching effects are observed in a very narrow temperature region, close to the critical temperature  $T_c$ , for a reduced value  $t = T/T_c \approx 0.95$ . In order to both increase the matching field and decrease the temperature where the effect is present, the period of the pinning structure should be reduced to less than 100 nm. This gives, in fact, the possibility to increase  $H_1$  up to 1 tesla or even higher. A reasonable method to achieve this goal is to use self-assembled substrates, such as, for example,  $\text{Al}_2\text{O}_3$  templates with characteristic features in the nanometric scale [15]. The pore diameter in  $\text{Al}_2\text{O}_3$  substrates could easily be varied in the range 25–200 nm with porosity (i.e. interpore spacing) around 50%, and this gives the possibility to achieve

matching fields of thousands of oersteds [15]. To prepare  $\text{Al}_2\text{O}_3$  substrates bulk Al [16], Al foils [17], and deposited thick Al films were used [15].

Very recently, another very promising material for self-assembled substrates and an optimum candidate for the Nb growth was proposed, namely, porous silicon (PS) [18]. PS is constituted by a network of pores immersed in a nanocrystalline matrix [19] and it is a material which offers a considerable technological interest in different fields, as for instance micro and optoelectronics [20] and gas sensing [21,22]. The diameter of pores,  $\phi$ , in PS can easily be varied from 200 nm down to 5 nm by using substrates with appropriate doping (n or p) and different regimes of anodization. The porosity, in fact, can be varied in the range 30–90% by adjusting parameters such as the acid solution, the anodizing current density and the illumination of the substrate during the anodization. The regularity of the pores arrangement, however, is of the order of 10% lower than the one observed in  $\text{Al}_2\text{O}_3$  templates obtained by electrochemical oxidation [23]. It has been demonstrated [18] that thin Nb films deposited on PS substrates can inherit their structure. The resulting samples then consist of porous Nb thin films with in plane geometrical dimensions,  $a_0$  and  $a_0$ , comparable with the superconducting coherence length,  $\xi(T)$ . In these samples, matching fields of the order of 1 Tesla were experimentally observed [18].

Aim of this work is to deepen the study of the matching effect in superconducting Nb thin films deposited on PS. Superconducting properties were investigated by transport measurements in the presence of magnetic fields applied perpendicularly to the samples surface, down to  $T = 0.52$ . As a consequence of the high density of the pore network, the  $(H, T)$  phase diagram presents a deviation from the classic linear dependence. This effect appears at the matching field  $H_1 = 1$  Tesla, a value larger than those typical of periodic pinning arrays obtained both by lithographic techniques and by using another kind of self-organized templates. Moreover a new effect related to the commensurability between the vortex lattice and the underlying pinning structure was found. It consists in the appearance of pronounced structures in the derivative of the  $R(H)$  curves,  $dR/dH$ , which can be observed in correspondence of the first matching field and its fractional values.

**Fabrication.** { Porous layers were fabricated by electrochemical anodic etching of n-type, 0.01 cm, monocrystalline silicon wafers. The electrochemical dissolution was performed in 48% water solution of  $\text{HF}$ , applying a current density of  $20 \text{ mA/cm}^2$ . The anodization time was chosen in the range of 0.5–4 min in order to get porous layers with a thickness ranging from 0.5 to 4  $\mu\text{m}$ . The pores extend on a surface of about  $1 \text{ cm}^2$ . The integral porosity was estimated by gravimetry to be of about 50% [24]. The resulting porous substrates have  $\phi = 10 \text{ nm}$  and  $a_0 = 40 \text{ nm}$ . For this lattice, if the formula

$H_1 = \phi/a_0^2$  for the square lattice is used, the expected first matching field is  $H_1 = 1.3$  Tesla.

Nb thin films were grown on top of the porous Si substrates in a UHV dc diode magnetron sputtering system with a base pressure in the low  $10^{-8}$  mbar regime and sputtering Argon pressure of  $3.5 \cdot 10^{-3}$  mbar. In order to reduce the possible contamination of the porous templates, the substrates were heated at 120 °C for one hour in the UHV chamber. The deposition was then realized at room temperature after the cooling of the substrates. Films were deposited at typical rates of 0.33 nm/s, controlled by a quartz crystal monitor calibrated by low-angle reflectivity measurements. Since the effect of the periodic template would be reduced when the film thickness,  $d$ , exceeds the pore diameter,  $\phi$ , [18] the Nb thickness was chosen to be 8.5 nm for the sample analyzed in this paper. A reference Nb thin film of the same thickness was grown on a non-porous Si substrate in the same deposition run.

**Experimental results and discussion.** { The superconducting properties were resistively measured in a  $^4\text{He}$  cryostat using a standard dc four-probe technique on unstructured samples. The critical temperature was defined at the midpoint of the  $R(T)$  transition curves. The value of the transition temperatures of the film grown on the porous substrate and of the reference sample in the absence of the magnetic field were  $T_c = 3.83 \text{ K}$  and  $T_c = 4.53 \text{ K}$ , respectively. The critical temperature depression in the case of the porous sample is consistent with what already reported in literature for films grown both on  $\text{Al}_2\text{O}_3$  [15] and on PS [18]. The first step for the characterization of the behavior of the porous Nb sample in the presence of perpendicular magnetic field is the determination of its  $(H, T)$  phase diagram. The temperature dependence of the perpendicular upper critical field,  $H_{c2?}$ , was obtained performing resistance vs. field,  $R(H)$ , measurements at fixed values of the temperature with a temperature stability of 1 mK.  $H_{c2?}$  was defined at the midpoint of each of the  $R(H)$  curves.

In Fig. 1 the  $(H, T)$  phase diagrams of the Nb thin films are shown. In general, the perpendicular upper critical field of superconducting films of thickness  $d$  obeys a linear temperature dependence,  $H_{c2?}(T) = (\phi_0/2\xi_{0k})(1 - T/T_c)$  [25].  $\xi_{0k}$  is the Ginzburg-Landau coherence length parallel to the sample surface at  $T = 0$ . The temperature dependence of  $\xi_k$  is  $\xi_k(T) = \xi_{0k}/\sqrt{1 - T/T_c}$ . Another superconducting parameter to be taken into account is the magnetic field penetration depth,  $\lambda$ , whose temperature dependence is  $\lambda(T) = \lambda_0/\sqrt{1 - T/T_c}$ , where  $\lambda_0$  is the penetration depth at  $T = 0$ .

The  $H_{c2?}(T)$  curve obtained for the Nb film deposited on porous Si template, reported in Fig. 1(a), presents some peculiarities, which indicate that the superconducting properties are influenced by the introduction of the porous array. In fact, if the  $H_{c2?}$  second derivative versus the temperature is plotted we can see that it changes its sign from positive to negative at  $H = 1.16$  Tesla. This field

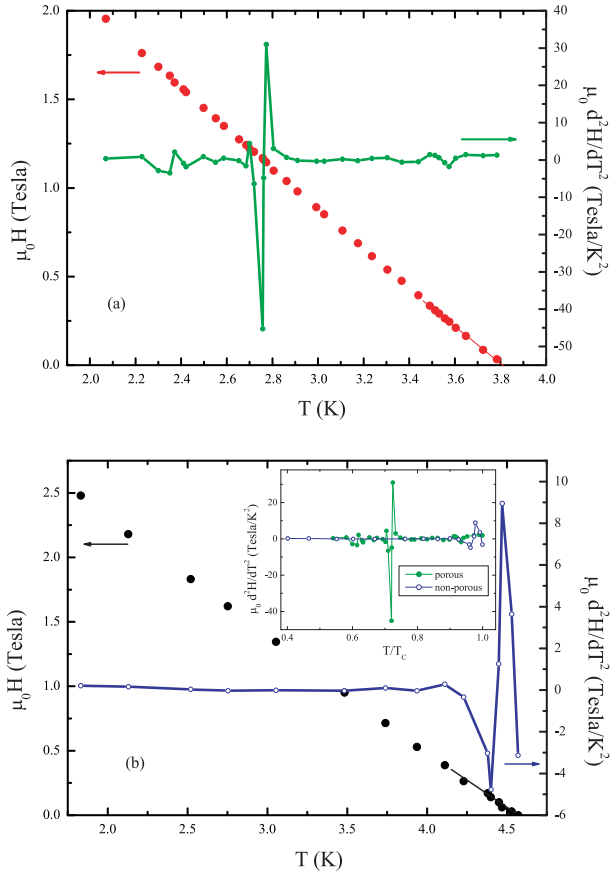


Fig. 1: Left scale: Perpendicular upper critical field  $H_{c2}$  vs. temperature of the Nb thin film with  $d_{Nb} = 8.5$  nm grown on (a) porous template and (b) non-porous reference substrate. The linear fits to the data close to  $T_c$  are also shown. Right scale:  $d^2H_{c2}/dT^2$  versus temperature. The inset shows the comparison between the second derivatives as functions of the reduced temperature of two samples, grown on the porous template (full circles) and on the non-porous template (open circles). (Color online).

value is very close to the nominal first matching field that we expect for the porous Si template,  $H_1 \approx 1.30$  Tesla, assuming a square porous array. This change in concavity was already reported in a previous study on the same kind of samples, and it was ascribed to the formation of a commensurate vortex structure [18]. From the measured value of  $H_1$  it follows that the period of the porous template is  $a = 42$  nm. In the following we will identify  $a_0 = 42$  nm. In Fig. 1 (b) is reported the  $H_{c2}(T)$  curve for the Nb reference film of the same thickness deposited on the non-porous template. As expected the  $H_{c2}(T)$  behavior is linear over the all temperature range and the  $H_{c2}$  second derivative versus temperature does not present any peculiarity except for a shallow peak near  $T_c$ . In the inset of Fig. 1 (b), for sake of comparison, the  $d^2H_{c2}/dT^2$  versus the reduced temperature is reported for both the Nb films, in order to point out the difference in their magnitude. As to the data close to  $T_c$  with the expression for

$H_{c2}(T)$  reported above, yields a value of the Ginzburg-Landau coherence length at  $T = 0$ ,  $\xi_0 = 9.1$  nm and  $\xi_0 = 9.5$  nm, resulting in a superconducting coherence length  $\xi_s = 5.8$  nm and  $\xi_s = 6.0$  nm, for the Nb porous sample and the Nb reference film, respectively. The values of  $\xi_0$  are significantly smaller than the BCS coherence length of Nb,  $\xi_0 = 39$  nm [26], indicating that our films are in dirty limit regime with an electron mean free path of  $l = 1.38 \xi_0 / \phi_0 \approx 3$  nm [27]. Since the film dimensions in the xy plane are larger than  $\xi_0(T)$ , the expression for  $H_{c2}(T)$ , reported above, is verified in the whole temperature range. The Ginzburg-Landau parameter,  $\kappa = \xi_0/\lambda$ , can be estimated using the expression  $\kappa = 0.72 \lambda_L/l = 9.6$ , where  $\lambda_L = 39$  nm is the London penetration depth of Nb [26]. Ratios of  $\xi_0/a = 0.2$  and  $\xi_0/a = 2.1$ , measured for  $a_0 = 42$  nm, are larger than in previous works [17,28] on perforated Nb samples, and indicate that we are in presence of individual vortex pinning [29]. Moreover, the pore diameter,  $\phi$ , in our PS template is comparable with the vortex core dimension at  $T = 0$ ,  $\xi_0$ . This means that the saturation number,  $n_s = \frac{2}{\phi} \xi_0(T)$ , defined as the maximum number of vortices that fits into a pore with diameter  $\phi$ , is less or equal to 1, so that each pore can trap only one fluxon [30]. Subsequently multiquanta vortex lattice [2] cannot be observed in our system.

Now we move to a more careful inspection of the  $R(H)$  curves of the Nb porous film. This will lead to the observation of a peculiar behavior of these transitions, whose analysis represents the main subject of this work. In Figs. 2 (a) and 2 (b)  $R(H)$  curves obtained for two different values of the temperature,  $T = 3.490$  K and  $T = 3.531$  K, respectively, are presented.

At first glance both the curves are rather smooth and do not present any structures or enlargements due, for example, to sample inhomogeneities. However if the dependence of the first derivative  $dR/dH$  versus the applied magnetic field is analyzed, some distinct features can be observed. In particular in both the curves a small local maximum is present at specific values of the magnetic field. Let's focus on the position where the bumps, as indicated by an arrow in Fig. 2, start to develop. The bumps in the first derivative reflect the presence of a small dip in the corresponding magnetic field dependence of the resistance  $R(H)$  at the same value of  $H$ . This effect was ascribed to a pinning enhancement when the period of the vortex structure is commensurate with the period of the antidots [31]. The bumps in the  $dR/dH$  appear indeed in our curves at values of the magnetic fields  $H_n$  when the magnetic flux threading each unit cell is equal to the flux quantum,  $\phi_0$ , or to fractional values of  $\phi_0$ . In Fig. 2 (a), where the  $R(H)$  measurement at  $T = 3.490$  K is shown, the peculiarity in  $dR/dH$  is, in fact, observed at  $H_{bump} = 0.126$  Tesla. The period of the vortex lattice at this field value is  $a^0 = 128$  nm, i.e. about three times the interpore spacing of this analyzed sample,  $a_0 = 42$  nm. Consequently this field value corresponds to one-ninth of the matching

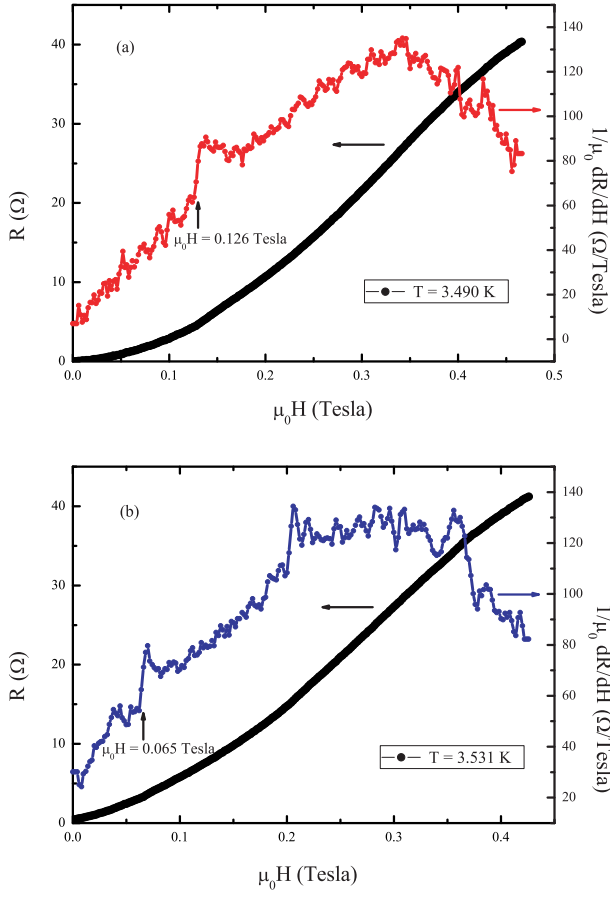


Fig. 2: Left scale:  $R(H)$  measurement at (a)  $T = 3.490$  K and (b)  $T = 3.531$  K. Right scale:  $dR/dH$  versus the applied magnetic field. In both panels the arrow indicates the field where the bump is present. (Color online)

field  $H_1/9 = 0.129$  Tesla. Similarly, in Fig. 2(b) where the  $R(H)$  measurement at  $T = 3.531$  K is shown, the bump in  $dR/dH$  develops at  $H_{\text{bump}} = 0.065$  Tesla. The period of the vortex array at this field is then  $a^0 = 178$  nm, which is about four times the inter-pore spacing of this sample. Consequently this field value corresponds to one-sixteenth of the matching field  $H_1/16 = 0.072$  Tesla. An additional bump structure is present at  $H = 0.2$  Tesla. However, this field value does not correspond to any commensurate vortex configuration (see discussion below) and does not survive repeating the measurement in the same temperature range. Many  $R(H)$  measurements at different temperatures have been performed and the behavior of all the corresponding  $dR/dH$  curves has been analyzed. A selection of these curves is reported in Fig. 3. Some of them have been obtained by sweeping the field upward and downward and no hysteresis has been detected.

For instance, the curves at  $T = 2.551$  K and  $T = 3.304$  K present a bump at  $H_{\text{bump}} = H_1$  and  $H_{\text{bump}} = H_1/4$ , respectively. By comparison a curve with no bump, measured at temperature  $T = 2.805$  K, is also shown. In all curves the fields at which the bumps are observed are re-

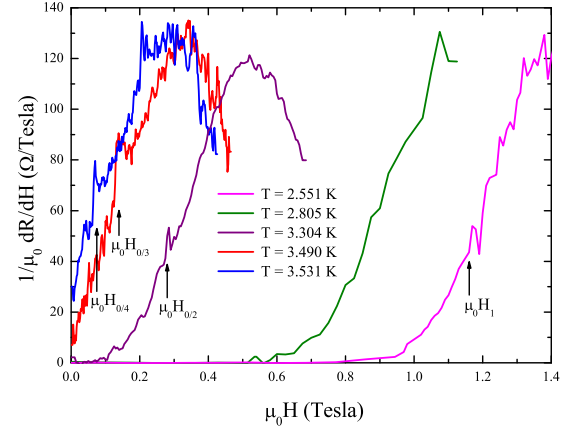


Fig. 3: First derivatives,  $dR/dH$ , as a function of the applied magnetic field at different temperatures. The arrows indicate the field where the bump is present for each temperature. (Color online)

lated to the first matching field through the relation:  $H = H_1/n^2$  with  $n = 1, \dots, 4$ . The temperatures at which bumps are observed, the corresponding fields and their values normalized to  $H_1$ , the  $s$  values, the vortex-vortex distances,  $a$ , and their values normalized to  $a_0$ , are summarized in Table 1.

We argue that the presence of the observed bumps in the  $dR/dH$  curves can be related to different vortex lattice arrangements made possible by the lattice of holes. The specific vortex lattice configurations occurring at the first matching field and at its fractional values are shown in Fig. 4.

In the case of  $H_{\text{bump}}/H_1 = 1$  a commensurate square vortex configuration is formed, where each pore is occupied by a fluxon and the side of this square array is just  $a_0 = 42$  nm. Increasing the temperature the vortices diameter ( $2s$ ) and their reciprocal distance increase, as reported in Table 1. When  $H_{\text{bump}}/H_1 = 1/4, 1/9$  and  $1/16$  a square vortex lattice is again obtained with  $a = 87$  nm,  $128$  nm and  $178$  nm, respectively. This means that the pores act as an ordered template of strong pinning centers, which is able to preserve the long range positional order of the flux lattice also at low fields value, i.e. at higher vortex spacing. As already pointed out the optimization of the vortex structures leads to the formation of larger square flux lattices with respect to the underlying artificial pinning array with the lattice constant exactly equal to  $na_0$ . The vortices tend to be placed as far from each other as possible due to the repulsive interaction between them and at the same time they want to follow the imposed square potential induced by the antidots. This constraint gives  $a = a_0 \sqrt{l^2 + k^2}$ , where  $l$  and  $k$  are integer numbers. Therefore, we should expect the fractional matching fields at  $H = H_{k=1} = a_0^2 = a_0^2 [l^2 + k^2]$

Table 1: Temperatures at which the bumps are observed, corresponding fields and their values normalized to  $H_{1,s}$  values at that temperature, vortex-vortex distances,  $a_{k=1}$ , and their values normalized to  $a_0 = 42$  nm.

T (K)	$H_{\text{bump}}$ (T)	$\frac{H_{\text{bump}}}{H_1}$	$s$ (nm)	$a_{k=1}$ (nm)	$\frac{a_{k=1}}{a_0}$
2.551	1.160	1	10.02	42.0	1.00
3.304	0.275	1/4	15.66	87.0	2.07
3.490	0.126	1/9	19.44	128.0	3.05
3.531	0.065	1/16	20.76	178.0	4.24

$= H_1 = (l^2 + k^2)$  [32]. We observed bumps at fractional matching fields  $H_{0=2}$ ,  $H_{0=3}$  and  $H_{0=4}$ . The other bumps expected from the equation above at fractional fields  $H_{k=1}$  with  $k \neq 0$  have not been observed. All the fields values at which the bumps in the  $dR/dH$  appear are shown as points of coordinates  $(H_{\text{bump}}, T)$  in Fig. 5.

In this figure the solid lines correspond to the matching fields of different order, as calculated assuming an inter-pore spacing  $a_0 = 42$  nm, through the formula  $H_1 = \frac{\Phi_0}{2a_0^2}$ . The dotted lines are obtained considering a deviation from the corresponding mean inter-pore distance of the order of 10% [18]. It is worth noticing that all the data fall into the range theoretically estimated, suggesting that the observed peculiarities in the  $R(H)$  curves can be indeed ascribed to commensurability effect between the porous structure of the Nb film and the vortex lattice. The distribution of the experimental points is consistent with the observation that a certain temperature dependence of the matching effect can be found for the case of short-range ordered templates [12]. We would also point out that the effect is observable in our sample only up to  $H = H_1$ , due to the very high value of the first matching field. The second matching field in fact is  $H_2 = 2H_1 = 2.32$  Tesla. From a linear extrapolation of the  $H_{c2}$  curve, it follows that in order to see at this field a bump in the  $dR/dH$  we should measure a  $R(H)$  curve at  $T = 1.73$  K, temperature which cannot be reached in our experimental setup. All the field values reported above have been calculated assuming a square lattice. The measured field values do not match with the ones calculated if a triangular array for the pores is considered. In fact, at  $T = 3.490$  K (see Fig. 2(a)) the structure in the  $dR/dH$  curve for a triangular lattice would have been observed at a field  $2\sqrt{3}$  times higher than  $H_{0=3} = 0.126$  Tesla, where no peculiar feature has been detected. This supports our assumption of considering a square lattice of holes in our system.

**Conclusions.** Matching effects have been reported for Nb thin film grown on porous silicon. Due to the extremely reduced values of the inter-pore distance the effect is present at fields values higher than 1 Tesla and down to reduced temperatures as low as  $T \approx 0.52$ . The commensurability manifests both in the  $(H, T)$  phase diagram and

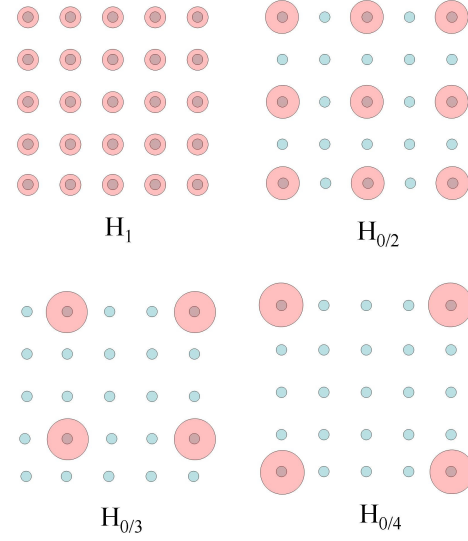


Fig. 4: Vortex lattice configurations occurring at the first matching field and its fractional values. Increasing the temperature the vortices diameter and their reciprocal distance increase, as reported in Table 1. Blue circles represent the holes, pink ones represent the vortices. (Color online)

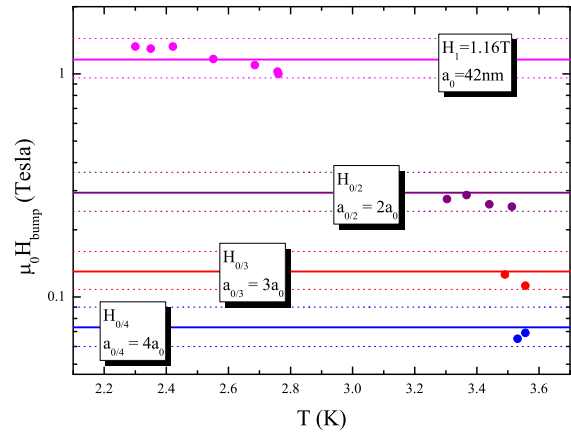


Fig. 5: The points of coordinates  $(H_{\text{bump}}, T)$  identify the values of the fields and temperatures at which bumps have been observed in the  $dR/dH$  curves at fixed temperatures. The solid lines correspond to the different matching field orders achieved with the inter-pore spacing  $a_0 = 42$  nm, while the dotted lines are obtained for as much as the regularity of the pore distance is achieved within the 10 percents of the average distance. (Color online)

in the  $R(H)$  transitions. The latter in particular reveal the formation of fractional matching states. As it was argued in many works the vortex configuration at fractional matching fields are characterized by striking domain structure and associated grain boundaries [33,34]. The presence of multiple degenerate states with domain formation at the fractional field, directly observed with scanning Hall probe microscopy [33], seems to be highly probable in our films. The reduced regularity of our templates, in fact, could be compensated by the formation of domain walls of different complexity. The particular domain configuration is of course a matter of energy balance between the cost in energy for the wall formation and the energy gain due to the vortex pinning.

## REFERENCES

- [1] Abrikosov A.A., *Sov. Phys. JETP*, **5** (1957) 1174.
- [2] Moshchalkov V.V., Baert M., Metlushko V.V., Rosseel E., Van Bael M.J., Temst K., and Bruynseraede Y., *Phys. Rev. B*, **57** (1998) 3615.
- [3] Hoffmann A., Prieto P., and Schuller Ivan K., *Phys. Rev. B*, **61** (2000) 6958.
- [4] Fiory A.T., Hebard A.F., and Somekh S., *Appl. Phys. Lett.*, **32** (1978) 73.
- [5] Lykov A.N., *Solid St. Commun.*, **86** (1993) 531.
- [6] Castellanos A., Wördenweber R., Ockenfuss G., Hart A.v.d., and Keck K., *Appl. Phys. Lett.*, **71** (1997) 7.
- [7] Mart n J.I., Velez M., Nogues J., and Schuller Ivan K., *Phys. Rev. Lett.*, **79** (1997) 1929.
- [8] Van Bael M.J., Temst K., Moshchalkov V.V., and Bruynseraede Y., *Phys. Rev. B*, **59** (1999) 14674.
- [9] Velez M., Mart n J.I., Villegas J.E., Hoffmann A., Gonzales E.M., Vincent J.L., and Schuller Ivan K., *J. Magn. Magn. Mater.*, **320** (2008) 2547.
- [10] Silhanek A.V., Van Look L., Jonckheere R., Zhu B.Y., Raedts S., and Moshchalkov V.V., *Phys. Rev. B*, **72** (2005) 014507.
- [11] Little W.A. and Parks R.D., *Phys. Rev. Lett.*, **9** (1962) 9.
- [12] Eisenmenger J., Oettinger M., Pfahler C., Plett A., Walther P., and Ziemann P., *Phys. Rev. B*, **75** (2007) 144514.
- [13] Kemmler M., Gurlich C., Sterck A., Pohler H., Neuhaus M., Siegel M., Kleiner R., and Koelle D., *Phys. Rev. Lett.*, **97** (2006) 147003.
- [14] Van de Vondel J., de Souza Silva C.C., Zhu B.Y., Morelle M., and Moshchalkov V.V., *Phys. Rev. Lett.*, **94** (2005) 057003.
- [15] Vinckx W., Vanacken J., Moshchalkov V.V., Matefi-Tempfli S., Matefi-Tempfli M., Michotte S., Piraux L., and Ye X., *Physica C*, **459** (2007) 5.
- [16] Prischepa S.L., Lynkov L.M., Lykov A.N., and Dedyu V.I., *Cryogenics*, **34** (1994) 851.
- [17] Welp U., Xiao Z.L., Jiang J.S., Vlasko-Vlasov V.K., Bader S.D., Crabtree G.W., Liang J., Chik H., and Xu J.M., *Phys. Rev. B*, **66** (2002) 212507.
- [18] Trezza M., Prischepa S.L., Cirillo C., Fittipaldi R., Sarno M., Sannino D., Ciambelli P., Hesselberth M.B.S., Lazarouk S.K., Dolbik A.V., Borisenko V.E., and Attanasio C., *J. Appl. Phys.*, **104** (2008) 083917.
- [19] Bisio O., Ossicini S., and Pavesi L., *Surf. Sci. Rep.*, **38** (2000) 1.
- [20] Collins R.T., Fauchet P.M., and Tischler M.A., *Phys. Today*, **50** (1997) 24.
- [21] Cheraga H., Belhousse S., and Gabouze N., *Appl. Surf. Sci.*, **238** (2004) 495.
- [22] Lysenko V., Perichon S., Remaki B., Champagnon B., and Barbier D., *J. Appl. Phys.*, **86** (1999) 6841.
- [23] Matefi-Tempfli S., Matefi-Tempfli M., and Piraux L., *Thin Solid Films*, **516** (2008) 3735.
- [24] Lazarouk S.K., Dolbik A.V., Labunov V.A., and Borisenko V.E., *Physics, Chemistry and Application of Nanostructures (World Scientific) 2007*, p. 223.
- [25] Tinkham M., *Introduction to Superconductivity (McGraw-Hill Inc) 1996*.
- [26] Buckel W., *Supraleitung*, 3rd edn. (Physik-Verlag, Weinheim) 1984.
- [27] Schmidt V.V., *The Physics of Superconductors*, edited by P. Müller and A.V. Ustinov (Springer, Berlin-Heidelberg) 1997.
- [28] Vinckx W., Vanacken J., Moshchalkov V.V., Matefi-Tempfli S., Matefi-Tempfli M., Michotte S., and Piraux L., *Eur. Phys. J. B*, **53** (2006) 199.
- [29] Brandt E.H., *Phys. Lett.*, **77A** (1980) 484.
- [30] Mkrtchyan G.S. and Schmidt V.V., *Zh. Eksp. Teor. Fiz.*, **61** (1971) 367. [*Sov. Phys. JETP* **34**, 195 (1972)].
- [31] Patel U., Xiao Z.L., Hua J., Xu T., Rosenmann D., Novosad V., Pearson J., Welp U., Kwok W.K., and Crabtree G.B., *Phys. Rev. B*, **76** (2007) 020508(R).
- [32] Baert M., Metlushko V.V., Jonckheere R., Moshchalkov V.V., and Bruynseraede Y., *Europhys. Lett.*, **29** (2) (1995) 157.
- [33] Field S.B., James S.S., Barentine J., Metlushko V., Crabtree G., Shtrikman H., Ilic B., and Brueck S.R.J., *Phys. Rev. Lett.*, **88** (2002) 6.
- [34] Grigorenko A.N., Bending S.J., Van Bael M.J., Lange M., Moshchalkov V.V., Fangohr H., and de Groot P.A.J., *Phys. Rev. Lett.*, **90** (2003) 23.